Design of High Efficiency Multi-GHz SiGe HBT Electro-Optic Modulator

Shengling Deng, Z. Rena Huang*, J. F. McDonald

Department of Electrical, Computer, and System Engineering, Rensselaer Polytechnic Institute, 110 8th Street, Troy, NY 12180, USA

**zrhuang@ecse.rpi.edu*

Abstract: We design and theoretically analyze a heterojunction bipolar transistor (HBT) electro-optic (EO) modulator with a composition graded SiGe base. The waveguide has a large cross-section of 1μm for ease of fiber alignment. At a base-emitter bias of V_{BE} = 2.5V, a π-phase shift requires 74.5μm interaction length for TM polarization at λ = 1.55μm. The total optical attenuation is 3.9dB to achieve a π-phase shift in this condition. This device is expected to operate at a switching speed of 2.4GHz.

OCIS codes: (130.4110) Modulator; (130.3120) Integrated optics devices; (230.2090) Electro-optic devices

References and links

1. Y. H. Kuo, Y. K. Lee, Y. Ge, S. Ren, J. E. Roth, T. I. Kamins, D. A. B. Miller, and J. S. Harris, "Strong quantum-confined Stark effect in germanium quantum-well structures on silicon," Nature **437**(7063), 1334–1336 (2005).
2. R. S. Jacobsen, K. N. Andersen, P. I. Borel, J. Fage-Pedersen, L. H. Frandsen, O. Hansen, M. Kristensen, A. V. Lavrinenko, G. Moulin, H. Ou, C. Peucheret, B. Zsigri, and A. Bjarklev, "Strained silicon as a new electro-optic material," Nature **441**(7090), 199–202 (2006).
3. C. Cocorullo, M. Iodice, I. Rendina, and P. M. Sarro, "Silicon thermo-optical micro-modulator with 700 kHz – 3 dB bandwidth," IEEE Photon. Technol. Lett. **7**(4), 363–365 (1995).
4. Q. Xu, B. Schmidt, S. Pradhan, and M. Lipson, "Micrometre-scale silicon electro-optic modulator," Nature **435**(7040), 325–327 (2005).
5. A. Liu, L. Liao, D. Rubin, H. Nguyen, B. Ciftcioglu, Y. Chetrit, N. Izhaky, and M. Paniccia, "High-speed optical modulation based on carrier depletion in a silicon waveguide," Opt. Express **15**, 660–668 (2007).
6. F. Y. Gardes, G. T. Reed, A. P. Knights, and G. Mashanovich, "Evolution of optical modulation using majority carrier plasma dispersion effect in SOI", Proc. of SPIE **6898**, 68980C–68980C–10 (2008).
7. A. Liu, R. Jones, L. Liao, D. Samara-Rubio, D. Rubin, O. Cohen, R. Nicolaescu, and M. Paniccia, "A high-speed silicon optical modulator based on a metal-oxide-semiconductor capacitor," Nature **427**(6975), 615–618 (2004).
8. A. Liu, "Announcing the world's first 40G silicon laser modulator", http://blogs.intel.com/research/2007/07/40g_modulator.php
9. Y. Jiang, W. Jiang, L. Gu, X. Chen, and R. T. Chen, "80-micron interaction length silicon photonic crystal waveguide modulator," Appl. Phys. Lett. **87**(22), 221105 (2005).
10. A. Cutolo, M. Iodice, A. Irace, P. Spirito, and L. Zeni, "An electrically controlled Bragg reflector integrated in a rib silicon on insulator waveguide," Appl. Phys. Lett. **71**(2), 199 (1997).
11. G. Coppola, A. Irace, M. Iodice, and A. Cutolo, "Simulation and analysis of a high-efficiency silicon optoelectronic modulator based on a Bragg mirror," Opt. Eng. **40**(6), 1076–1081 (2001).
12. C. A. Barrios, V. Rosa de Almeida, and M. Lipson, "Low-power-consumption short-length and high-modulation-depth silicon electrooptic modulator," J. Lightwave Technol. **21**(4), 1089–1098 (2003).
13. X. Xiao, J. C. Sturm, K. K. Goel, and P. V. Schwartz, "Fabry-Perot optical intensity modulator at 1.3μm in silicon," IEEE Photon. Technol. Lett. **3**(3), 230–231 (1991).
14. M. Y. Liu, and S. Chou, "High-modulation-depth and short-cavity-length silicon Fabry-Perot modulator with two grating Bragg reflectors," Appl. Phys. Lett. **68**(2), 170 (1996).
15. C. A. Barrios, V. R. Almeida, R. Panepucci, and M. Lipson, "Electrooptic Modulation of Silicon-on-Insulator Submicrometer-Size Waveguide Devices," J. Lightwave Technol. **21**(10), 2332–2339 (2003).
16. S. Manipatruni, Q. Xu, B. Schmidt, J. Shakya, and M. Lipson, "High Speed Carrier Injection 18Gb/s Silicon Micro-ring Electro-optic Modulator," in *Proceedings of Lasers and Electro-Optics Society* (IEEE, 2007), pp.537–538.
17. R. D. Lareau, L. Friedman, and R. A. Soref, "Waveguided electro-optical intensity modulation in a Si/GexSi1-x/Si heterojunction bipolar transistor," Electron. Lett. **26**(20), 1653–1655 (1990).
18. A. Cutolo, M. Iodice, P. Spirito, and L. Zeni, "Silicon Electro-Optic Modulator Based on a Three Terminal Device Integrated in a Low-Loss Single-Mode SOI Waveguide," J. Lightwave Technol. **15**(3), 505–518 (1997).

#110744 - $15.00 USD Received 29 Apr 2009; revised 10 Jul 2009; accepted 13 Jul 2009; published 20 Jul 2009

19. S. J. McNab, N. Moll, and Y. A. Vlasov, "Ultra-low loss photonic integrated circuit with membrane-type photonic crystal waveguides," Opt. Express **11**, 2927–2939 (2003).
20. R. A. Soref, and B. R. Bennett, "Kramers-Kronig analysis of electro-optical switching in silicon," SPIE Integr. Opt. Circuit Eng. **704**, 32–37 (1986).
21. S. M. Sze, and K. K. Ng, *Physics of Semiconductor Devices* (John Wiley & Sons, Inc, 2007), Chap. 5.
22. R. A. Soref, J. Schmidtchen, and K. Petermann, "Large Single-Mode Rib Waveguides in GeSi-Si and Si-on-SiO_2," IEEE J. Quantum Electron. **27**(8), 1971–1974 (1991).
23. A. Sciuto, S. Libertino, A. Alessandria, S. Coffa, and G. Coppola, "Design, Fabrication, and Testing of an Interated Si-Based Light Modulator," J. Lightwave Technol. **21**(1), 228–235 (2003).
24. C. E. Png, G. T. Reed, R. M. H. Atta, G. Ensell, and A. G. R. Evans, "Development of Small Silicon Modulators in SOI," Proc. SPIE **4997**, 190–197 (2003).
25. L. Liao, D. Samara-Rubio, M. Morse, A. Liu, D. Hodge, D. Rubin, U. D. Keil, and T. Franck, "High Speed Silicon Mach-Zehnder Modulator," Opt. Express **13**(8), 3129–3135 (2005).
26. Q. Xu, S. Manipatruni, B. Schmidt, J. Shakya, and M. Lipson, "12.5 Gbit/s Carrier-injection-based silicon microring silicon modulators," Opt. Express **15**, 430–436 (2007).
27. S. Manipatruni, Q. Xu, and M. Lipson, "PINIP based high-speed high-extinction ratio micron-size silicon electro-optic modulator," Opt. Express **15**(20), 13035–13042 (2007).
28. F. Y. Gardes, K. L. Tsakmakidis, D. Thomson, G. T. Reed, G. Z. Mashanovich, O. Hess, and D. Avitabile, "Micrometer size polarisation independent depletion-type photonic modulator in Silicon On Insulator," Opt. Express **15**(9), 5879–5884 (2007).
29. S. Deng, Z. R. Huang, J.-R. Guo, J. F. McDonald, and R. P. Kraft, "Numerical Investigation of a SiGe HBT Electro-optic Modulator," in *proceedings of IEEE/LEOS Winter Topicals Meeting Series*, 14–15, (2009)
30. W. M. J. Green, M. J. Rooks, L. Sekaric, and Y. A. Vlasov, "Ultra-compact, low RF power, 10Gb/s silicon Mach-Zehnder modulator," Opt. Express **15**(25), 17106–17113 (2007).
31. Y. Taur, and T. H. Ning, *Fundamentals of Moerdern VLSI Devices* (Cambridge University Press, 1998), Chap. 6.

1. Introduction

Development of integrated electro-optic (EO) modulators with high speed, small footprint, low power, and compatibility with silicon fabrication processes is one of the challenges for building silicon-based integrated optical networks. In the past few years, extensive research has been performed in novel silicon EO modulators. For example, strained Ge/SiGe multiple quantum wells (MQW) [1] using quantum-confined Stark effect (QCSE), and strained Silicon with the Pockels effect [2] have been explored. However, these modulators are either immature in processing or of extremely low efficiency. Free carrier dispersion and the thermo-optic effect are possible mechanisms to create index modulation in silicon. The thermo-optic effect is rather slow with a modulation frequency only up to 1MHz [3]. Therefore, free carrier dispersion is the primary mechanism utilized in silicon EO modulators with gigahertz bandwidth and above.

Various electrical structures of free carrier dispersion based EO modulator have been explored in the past two decades. If possible, a device that is already in production for other applications is preferable to relying upon a totally new device due to the cost of introduction of new technology. According to how the free carrier plasma is generated, elementary structures can be categorized into three types: forward biased PIN diodes [4], reverse biased PN diodes [5,6], and Metal-Oxide-Semiconductor (MOS) capacitors [7]. For forward PIN diodes, the injection of minority carriers in the intrinsic region gives rise to a large refractive index modulation. This in turn leads to high modulation efficiency and small device footprint. However, forward PIN is typically slow because the injection of minority carriers is a slow process. For reverse biased PN diodes, the depletion of the majority carrier contributes to the refractive index modulation. It is a fast process with a delay characterized by the majority carrier relaxation time. The major drawback of the reverse biased EO modulator is its low modulation efficiency, since the refractive index modulation depth is limited by the background doping. For the MOS capacitor based EO modulators, the refractive index modulation is achieved through majority carrier accumulation, and it is thus an intrinsically fast device. However, the modulation efficiency is even lower because the thickness of the accumulated carriers is extremely thin. As a result, the MOS based EO modulator requires an active waveguide of several millimeters long for a phase shift of π. Traveling wave electrode design can greatly improve modulation efficiency. The fastest traveling wave EO modulator based on reverse biased PN structure has a demonstrated bit rate at 40Gbps [8]. The propagation of RF signal and optical wave along the long dimension of this type of device

#110744 - $15.00 USD Received 29 Apr 2009; revised 10 Jul 2009; accepted 13 Jul 2009; published 20 Jul 2009

must be such that the wavefronts of these two waves move at the same speed in tandem. This poses a design challenge since the speed synchronization is very difficult for microwave propagation in the transmission line and optical wave propagation in the dielectric waveguide.

In addition to exploring new electrical structures, the design of optical structures is another research focus. Photonic crystal (PC) waveguide [9] utilizing slow light effect, and resonant structures, such as distributed Bragg reflector [10–12], Fabry-Perot (FP) resonators [13–15], and ring resonator [4] are attractive in certain applications. An EO modulator incorporating ring resonator with diameter of 12μm has demonstrated a date rate of 18Gb/s [16]. The high bit rate was achieved because the transmission spectrum in this structure is very sensitive to carrier density change. However, for the same reason, this type of EO modulator is ultra sensitive to variations including temperature, bias voltage, and working wavelength. Additionally, one desires a low-Q structure to maintain a wider bandwidth.

In this paper, we propose a novel EO modulator that consists of a heterojunction bipolar transistor (HBT) with Si_xGe_{1-x} graded-base. The SiGe HBT EO modulator was first suggested by R.D.Lareau, et al [17] in 1990, in which the germanium composition was constant. Due to limitations in SiGe processing, it was not until 1992 that the composition graded SiGe HBT became available in commercial BiCMOS production line. The graded base SiGe HBT device benefits from a built-in electric field induced by the varying bandgap difference between the germanium and the silicon. An adjustable bandgap of Si_xGe_{1-x} can greatly enhance the device speed and offer many new design options for performance improvement in a HBT device. Of particular interest is the ability to trade HBT current gain enhancements for higher base doping, and lower base resistance.

The operation of an EO modulator with three terminals was first explored on bipolar mode FET (BMFET) [18], in which the lightwave was weakly guided by small index contrast between the intrinsic silicon and the heavily doped silicon. The BMFET EO modulator was long in active region and slow in speed. However, by principle the third terminal in an EO modulator can provide an additional freedom in manipulation of the electric field to maximize the overlap between the carrier plasma and the optical field in the waveguide. In this paper, we will show through our theoretical investigation that a phase shift of π can be achieved within an interaction length of 74.5μm. To our knowledge, the proposed HBT EO modulator is the *smallest* silicon-based EO modulator that works at GHz bandwidth without using any resonant structure. Among demonstrated GHz EO modulators either with PN or PIN structure, the cross-section of the rib waveguide is exclusively in submicron scale. A large waveguide cross-section (> 1μm) designed in this work can alleviate the complexity of light coupling from a fiber to the chip [19]. The trade-off of large cross-section is reduced switching speed due to longer carrier transit time across the base. In MOS EO modulator, the index modulation is obtained only in a thin layer consisting of inversion carriers; whereas the index modulation in a HBT is extended from the base to the collector and emitter region due to large carrier injection, leading to an increased overlap between the optical wave and the free carrier plasma. This thickness can be several 10's of nanometers to 100 nanometers.

2. Device structure

The EO modulator of this research incorporates a SiGe HBT with graded base as its electrical structure, and the Mach-Zehnder interferometer (MZI) as its optical structure to convert phase modulation into intensity modulation. One of the MZI arms is controlled by the HBT and the other one is for reference. The cross-section of a simplified device model used in the theoretical calculation is sketched in Fig. 1. The optical beam is coupled into the HBT from one facet and propagates along the z-axis. The designed HBT EO modulator has a vertical structure, which is prevalent in modern technology. The significance of vertical HBT in modern technology is that the emitter and the base widths are free from lithography limit, making ultra-high speed possible.

#110744 - $15.00 USD Received 29 Apr 2009; revised 10 Jul 2009; accepted 13 Jul 2009; published 20 Jul 2009

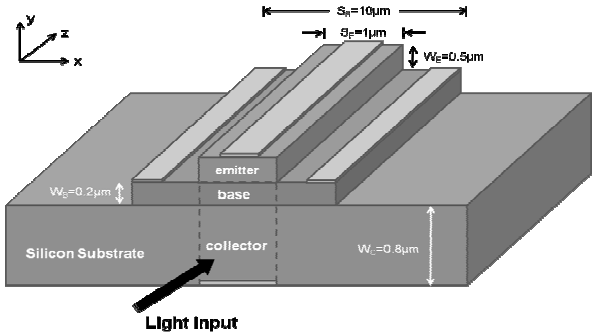

Fig. 1. 3D Schematic of the HBT EO modulator (not drawn to scale)

In our model, the emitter region is made of heavily doped n-type poly-silicon with a peak doping concentration of ~2×10^{20}cm^{-3}. The emitter contact is placed on the top of the device. The base region consists of a p-type $Si_{1-x}Ge_x$ epi-layer with x varying from 0% at the base-emitter junction to 20% at the base-collector junction. The active area of the base region is underneath the emitter, which is termed as intrinsic base. The intrinsic base has a peak doping concentration of 2×10^{19}cm^{-3} and is electrically connected through heavier doped extrinsic base regions with p-type doping (~10^{20}cm^{-3}) from both sides. This arrangement in a bipolar device targets at minimizing the base contact resistance as well as series resistance. The collector region is n-type doped at ~5×10^{17}cm^{-3}. An additional n^+ region, or the sub-collector, is buried at the bottom. The sub-collector is to reduce the contact resistivity to the collector terminal. In a real HBT device, the collector region is brought to the top metal layer via a reach-through structure. For the analysis of the electrical characteristics of the HBT, we place the collector contact at the bottom for simplicity. We assume that the waveguide is covered by an overglass SiO_2 (n_{SiO2} = 1.45) layer and the bottom is confined by a SiO_2 layer as well. The bottom SiO_2 can be introduced by substrate thinning followed by oxidization, or using Silicon on Insulator (SOI) technology. The large refractive index contrast between the silicon layer and the SiO_2 layer provides a strong optical confinement. The refractive index of intrinsic silicon is taken as n_{Si} = 3.42 in this work, while the $Si_{1-x}Ge_x$ refractive index is calculated from $n_{Si(1-x)Gex} = 3.42 + 0.37x + 0.22x^2$. The change of the refractive index in silicon as a result of free carrier plasma effect follows the well-known equations derived from Kramers-Kronig relation by R.A.Soref and B.R.Bennett [20]:

$$\begin{cases} \Delta n = \Delta n_e + \Delta n_h = -\left[8.8\times10^{-22}\Delta N_e + 8.5\times10^{-18}\left(\Delta N_h\right)^{0.8} \right] \\ \Delta \alpha = \Delta \alpha_e + \Delta \alpha_h = 8.5\times10^{-18}\Delta N_e + 6.0\times10^{-18}\Delta N_h \end{cases} \quad (1a)$$

$$\begin{cases} \Delta n = \Delta n_e + \Delta n_h = -\left[6.2\times10^{-22}\Delta N_e + 6.0\times10^{-18}\left(\Delta N_h\right)^{0.8} \right] \\ \Delta \alpha = \Delta \alpha_e + \Delta \alpha_h = 6.0\times10^{-18}\Delta N_e + 4.0\times10^{-18}\Delta N_h \end{cases} \quad (1b)$$

where Δn is the change of refractive index, and ΔN is the change of carrier density. The subscript "e" and "h" denotes the property change caused by electrons and holes, respectively. Equation (1)(a) and 1(b) corresponds to λ = 1.55μm and λ = 1.3μm, accordingly.

The complete doping profile at the device center along the y-direction is shown in Fig. 2.

#110744 - $15.00 USD Received 29 Apr 2009; revised 10 Jul 2009; accepted 13 Jul 2009; published 20 Jul 2009

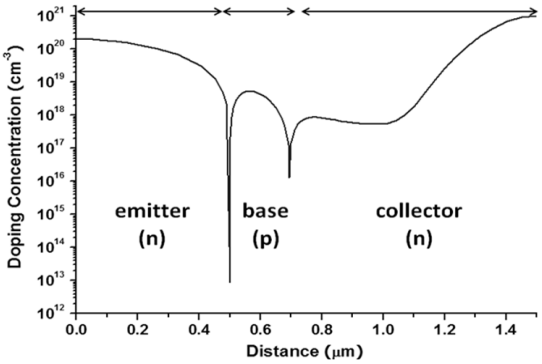

Fig. 2. Doping profile through the device center

Similar to PIN based EO modulator, the free carrier plasma effect in a HBT EO modulator is also produced by carrier injection. The injection can take place at emitter-base junction and/or the base-collector junction, depending on bias conditions. Elaboration on carrier injection behavior is presented in section 3.

In the PIN EO modulator, carrier injection is solely governed by minority carrier diffusion, which is a slow process; whereas for the HBT EO modulator, the built-in electric field in the base effectively reduces the electrons transit time. Therefore, HBT EO modulator is expected to work much faster. The built-in electric field also permits heavy doping in the base, which is a design not possible in homojunction bipolar device because the electron mobility greatly suffers from strong scattering. In addition, high emitter injection ratio enabled by the bandgap discontinuity ΔE_g at the emitter-base heterojunction is another reason why the base of HBT can have a high doping. Advantages of high doping in the base include less current crowding effect and smaller RC delay. It is worth noting that the base thickness favors high speed when small, but favors phase modulation efficiency when thick.

The HBT EO modulator is analyzed according to the following procedure: we first compute the carrier distribution throughout the device using a 2D device simulation package MEDICI; we then convert the 2D carrier distribution into refractive index profile through Eq. (1); next, we verify the single mode condition using both effective index method (EIF) and RSoft BeamProp CAD tool based on beam propagation method (BPM); finally, we import the refractive index data into BeamProp for mode computation. The EO modulation efficiency and the mode loss are calculated based on the effective index information. A MEDICI transient analysis is also performed to evaluate device switching performance.

3. Electrical and optical analysis

The proposed HBT EO modulator, as a three-terminal device, allows more options to control the carrier distribution in the device. In this research, we chose the common-emitter configuration, or more specifically, we maintain a reverse bias V_{CE} between the collector and the emitter, and apply a voltage at the base terminal. In the following DC characteristics investigation, we sweep the base bias V_{BE} from 0V up to 3.0V with a 0.5V step, while keeping a constant V_{CE} = 1.5V.

3.1 Carrier distribution

A bipolar transistor consists of two PN junctions, namely, the emitter-base junction and the base-collector junction. The injected electron density in the vicinity of the emitter-base junction can be expressed as [21]

$$n(0) = n_{p0} \exp\left[q\left(V_{BE} - \Delta V_{BE}\right) / \left(nkT\right)\right] \tag{2}$$

where n_{p0} is the electron density in the base at equilibrium, V_{BE} is the applied emitter-base bias, ΔV_{BE} is the voltage dropped on the series resistances in the quasi-neutral regions, and n is

#110744 - $15.00 USD Received 29 Apr 2009; revised 10 Jul 2009; accepted 13 Jul 2009; published 20 Jul 2009

an ideality factor. The hole injection in the emitter follows a similar relation, except that n_{p0} is replaced by p_{n0}. The equilibrium carrier concentration n_{p0} and p_{n0} in the heavily doped emitter and the base are larger than their nominal values due to bandgap narrowing effect [21]. As a result, increased minority carrier injections in the emitter (~50 times higher) and the base (~7 times higher) need to be taken account in the simulation.

With V_{BE} ramping up from 0V to 3.0V, the HBT operation mode shifts from cutoff to forward-active, and eventually to saturation. The energy band diagrams for thermal equilibrium condition, V_{BE} = 0V, 1.0V, and 2.5V are shown in Fig. 3. The Fermi level at thermal equilibrium condition is chosen as the reference point of the potential energy. The gradual energy bandgap narrowing in the base is the result of monotonic increase of germanium composition from the emitter side to the collector side. The conduction band bending establishes a built-in electric field that is favorable to the transport of electrons in the base. At V_{BE} = 0V, no carrier injection takes place at the emitter-base junction, though a constant bias V_{CE} = 1.5V set the device off the equilibrium. Thus, the device is in its "OFF" state. At moderate to high V_{BE} bias, as shown in Fig. 3 (c) and (d), the potential barrier at the emitter-base junction is reduced considerably, which allows the electrons from the emitter injected to the collector through the thin base region. This corresponds to the "ON" state. At high V_{BE} bias, the slope of the energy band bending is reduced at the base-collector interface due to Kirk effect.

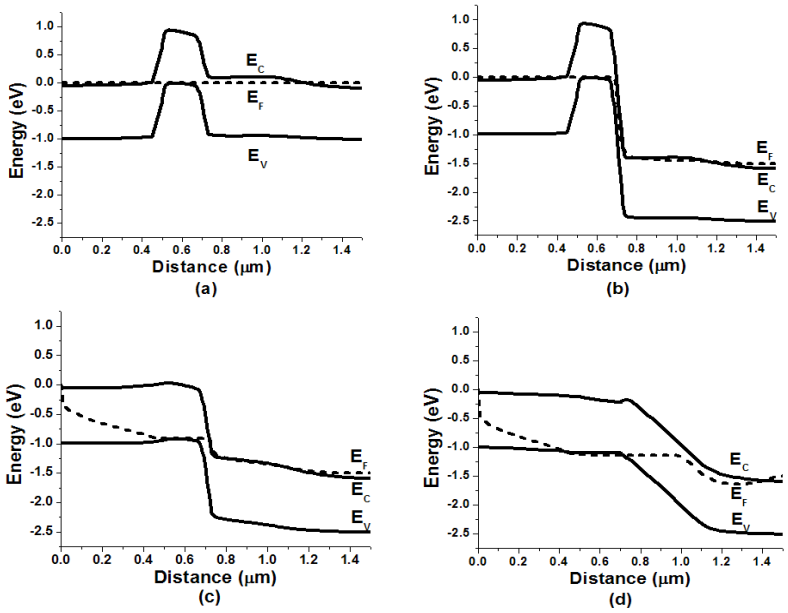

Fig. 3. Energy band diagram along *y*-axis at the device center under (a) Equilibrium condition, (b) No injection (V_{BE} = 0V, V_{CE} = 1.5V) from emitter to base, (c) Low injection (V_{BE} = 1.0V, V_{CE} = 1.5V), and (d) high injection (V_{BE} = 2.5V, V_{CE} = 1.5V) condition.

The carrier distribution at the middle of the device (along *y*-direction) is plotted in Fig. 4. When V_{BE} is below the threshold (~0.7V), carrier injection throughout the device is negligible, thus the free carrier plasma effect is minimal. Once V_{BE} is biased beyond 0.7V, obious electron injection from the emitter to the base is observed. The injected electrons move across the base and are finally collected in the collector. Similar injection takes place for the holes from the base side to the emitter side; therefore, the free carrier plasma also forms in the emitter. However, due to the previously mentioned bandgap offset ΔE_g, the hole injection level is much lower than the electron injection with a difference proportional to $\exp(-\Delta E_g/kT)$.

As we can see from Eq. (2), the carrier injection process follows an exponential relation to V_{BE}. Therefore, higher V_{BE} is the key to higher carrier density change, and thus higher phase

#110744 - $15.00 USD Received 29 Apr 2009; revised 10 Jul 2009; accepted 13 Jul 2009; published 20 Jul 2009

modulation efficiency. To achieve the best efficiency, the HBT device needs to work in saturation mode, which requires $V_{BE} > V_{CE} = 1.5$V. In this condition, we find from Fig. 4 (a) that the injected electron density is above the base doping level. As the consequence of charge neutrality requirement in the base, a significant hole density increase is observed. On the collector side, both electron and hole density increase slightly in the region immediately close to the base-collector junction. The increase in electron density indicates the amount of electrons entering the collector is greater than collector background doping. Similarly, the increase of hole density in the collector is also required by charge neutrality. This hole density increase in collector is equivalent to a widened base. In summary, when the HBT device is biased into saturation mode, strong electron and hole plasmas will generate in the base and its nearby regions. Thinner bases enhance speed, but reduce the volume of the carriers and their contribution to the index change. The extension of the free carrier plasma region beyond the base of the HBT is favorable, though weak, for the enhancement of modulation efficiency. But this also comes at the cost of speed.

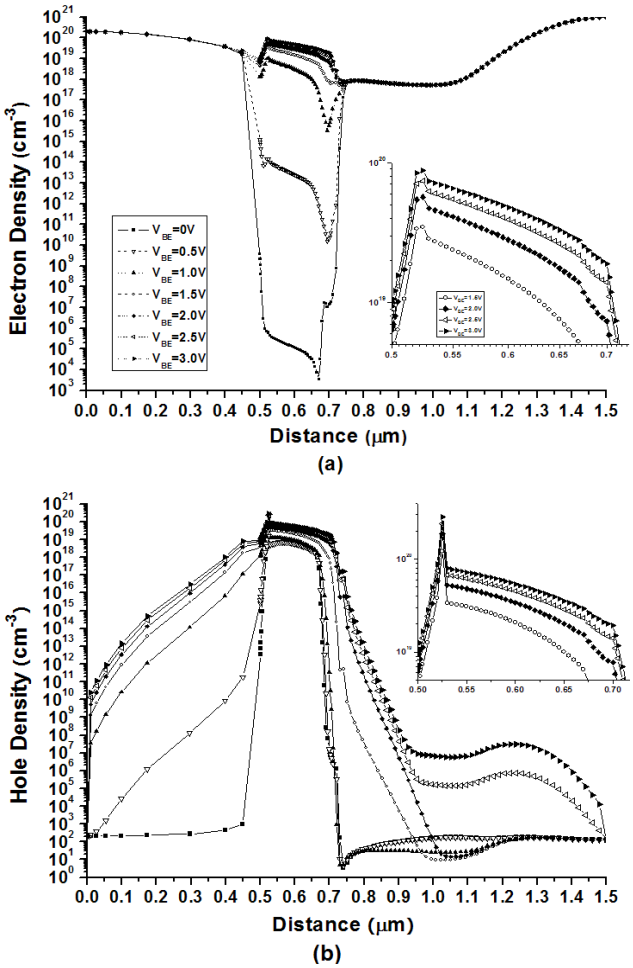

Fig. 4. One-dimensional carrier density plot along *y*-axis at device center for (a) electrons, and (b) holes (insets for locations between 0.5μm to 0.7μm at V_{BE} = 1.5V to 3.0V)

In the case of large V_{BE}, high-level injection effect and the parasitic series resistances effect have to be taken into consideration in choosing the working point. These two effects lead to a clamped injection level, because a significant portion of the increased voltage drops in the quasi-natural regions in this condition, instead of across the emitter-base junction. The

#110744 - $15.00 USD Received 29 Apr 2009; revised 10 Jul 2009; accepted 13 Jul 2009; published 20 Jul 2009

carrier density saturation can be clearly observed in Fig. 4. In other words, at high V_{BE}, a further increase in voltage only bring small extra increase to free carrier density; thereby an upper limit in the EO modulation efficiency is anticipated.

As we will elaborate in the following sections, the strong carrier density change at high V_{BE} also has an impact on waveguide properties, including mode distortion and possible cutoff of the fundamental mode.

3.2 Two-dimensional carrier distribution and refractive index contour

In section 3.1, a 1D carrier distribution at the center of the HBT device is plotted and discussed. However, the carrier distribution in the HBT is highly non-uniform in the lateral direction. This is because the series resistance in the intrinsic base is proportional to current path length. In the middle of the device where the current path is the longest, the resistance is the largest; near the intrinsic base edge, the resistance has the smallest value. As a result of the position dependent resistance, the current crowds at the edge of the intrinsic base and the emitter. We convert the 2D carrier distribution into refractive index map according to Eq. (1), and plot it in Fig. 5 for λ = 1.55μm at a few bias points. The current crowding effect is evident in this 2D refractive index contour. For the equilibrium condition, as is shown in Fig. 5 (a), the refractive index in the intrinsic base is higher than that in the extrinsic base, which is an outcome of the doping difference. A vertical index gradient is also observed. In the emitter, the gradient is a consequence of non-uniform doping profile; while in the base, it is primarily due to the germanium composition gradient. Although the doping profile in the HBT causes a higher refractive index in the intrinsic base than the extrinsic base at equilibrium, the free carrier plasma effect at high voltage can result in substantial refractive index decrease, and as a result, makes the intrinsic base index lower than that of the neighboring extrinsic base areas. This effect can be found in Fig. 5 (c). The non-uniform index distribution with reduced index in the waveguide center region could strongly alter the mode profile compared to the equilibrium condition, and lead to optical field expansion towards the slab regions. This phenomenon will be discussed next.

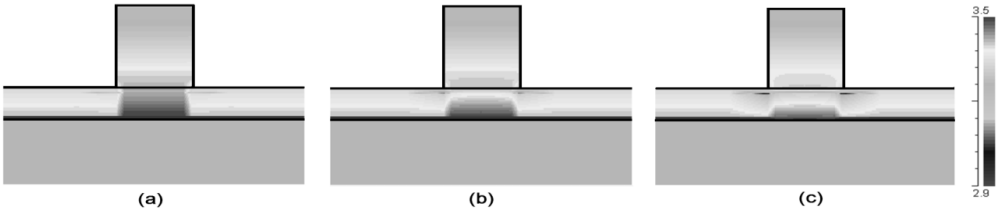

Fig. 5. Refractive index profile for λ = 1.55μm with V_{BE} = (a) 0V (b) 1.5V (c) 2.5V

3.3 Optical mode and modulation efficiency

The eigenmode in the HBT EO modulator waveguide is solved using Rsoft BeamPROP. Since this is not a mode coupling waveguide, we chose to use the semi-vector option to analyze the TE and the TM mode separately.

3.3.1 Verification of single mode condition

We first verify that the waveguide in this work satisfies single mode condition. For SOI wafers, a single mode rib waveguide usually needs to be as small as a few hundred nanometers in dimension. However, Soref et al. [22] provided a guideline for designing a single mode rib waveguide whose dimensions can be up to a few microns. Although the waveguide explored here is not a strict rib/ridge waveguide - due to the finite dimension of S_B in the base - we can still employ Soref's rule to check two extreme conditions as a start. Figure 6 (a) shows the sketch of the cross-section of a rib waveguide with the parameters *a*, *b*, and *r* defined as the same as those in [22]. The notation λ_0 refers to the free-space wavelength. In Fig. 6 (b), the simplified HBT structure of our design in analogy to a standard rib

#110744 - $15.00 USD Received 29 Apr 2009; revised 10 Jul 2009; accepted 13 Jul 2009; published 20 Jul 2009

waveguide is plotted. When S_B = 1μm as the base is aligned with the emitter width, or S_B is practically infinite, the HBT waveguide retrogrades to a standard rib waveguide with b = 0.484 for λ = 1.55μm (or b = 0.577 for λ = 1.3μm) and a/b = 0.667 according to our HBT parameters. When S_B = 1μm, the rib waveguide parameter r is 0.533, while when S_B approaches infinite, r is 0.667. The single mode regimes are calculated and plotted in Fig. 6 (c). The calculation suggests that single mode condition holds for all cases.

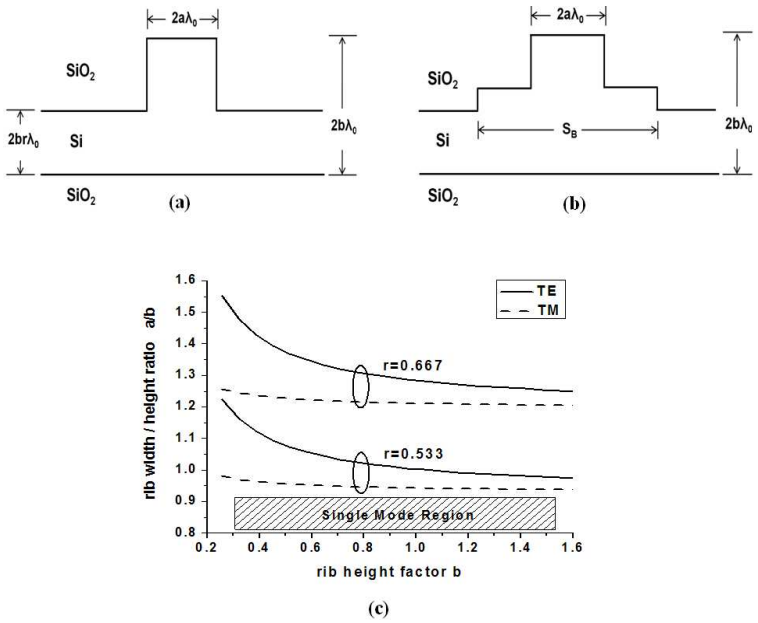

Fig. 6. (a) Cross-section of a standard rib waveguide, (b) Cross-section of a HBT waveguide structure, and (c) Single mode region for SiO_2/Si/ SiO_2 with r = 0.667 and 0.533.

In the above analysis, we neglected the index deviation caused by the SiGe base layer in the rib waveguide. This should not be a problem considering the small index difference between SiGe and silicon compared to the index contrast between silicon and SiO_2. However, if S_B does not fit into the above two situations, chances are higher order modes can be supported in the waveguide. Due to the requirement of placing base electrodes, S_B needs to be much larger than 1μm. Therefore, we need to determine the proper S_B range in which the waveguide exhibits similar properties as the second case (large S_B). We searched for the first order mode cutoff condition by scanning S_B in the range of 5μm to 13μm with a 0.5μm step. The simulation results for λ = 1.55μm indicate that the first order is cut off at S_B = 7.5μm for TE mode and S_B = 8.5μm for TM mode. At λ = 1.3μm, S_B is greater than 7.5μm for TE mode and 8μm for TM mode. Thus, the proposed HBT waveguide is of single mode.

3.3.2 Mode profile and interaction length for π-phase shift (L_π)

The eigenmode profiles for λ = 1.55μm are plotted in Fig. 7 at three different V_{BE} biases. The TM mode generally exhibits a better confined profile than the TE mode. Since the free carrier plasma is formed in the center of the device, a more compact mode profile of the TM mode implies a larger overlap integral of the electric field with the modified refractive index area. For TM mode, the E_y field contour maintains its general shape as V_{BE} increases, although spatial expansion is shown along the x-direction. For TE mode, the E_x field shows a more complicated behavior with the increase of V_{BE}, in which the peak of the electric field splits and drifts from the rib region to the nearby slab regions. In the refractive index discussion in section 3.2, we pointed out the drastic refractive index decrease in the rib region at high V_{BE} due to strong carrier injection. As a result, the rib region loses confinement of the electric field in the lateral direction, which gives rise to what is shown in Fig. 7 (c). At V_{BE} = 2.5V, a

#110744 - $15.00 USD Received 29 Apr 2009; revised 10 Jul 2009; accepted 13 Jul 2009; published 20 Jul 2009

dumbbell shaped mode profile appears in the TE mode profile. Since the electric field does not have a node in the waveguide center, the dumbbell shaped electric field should still be the fundamental mode of the waveguide.

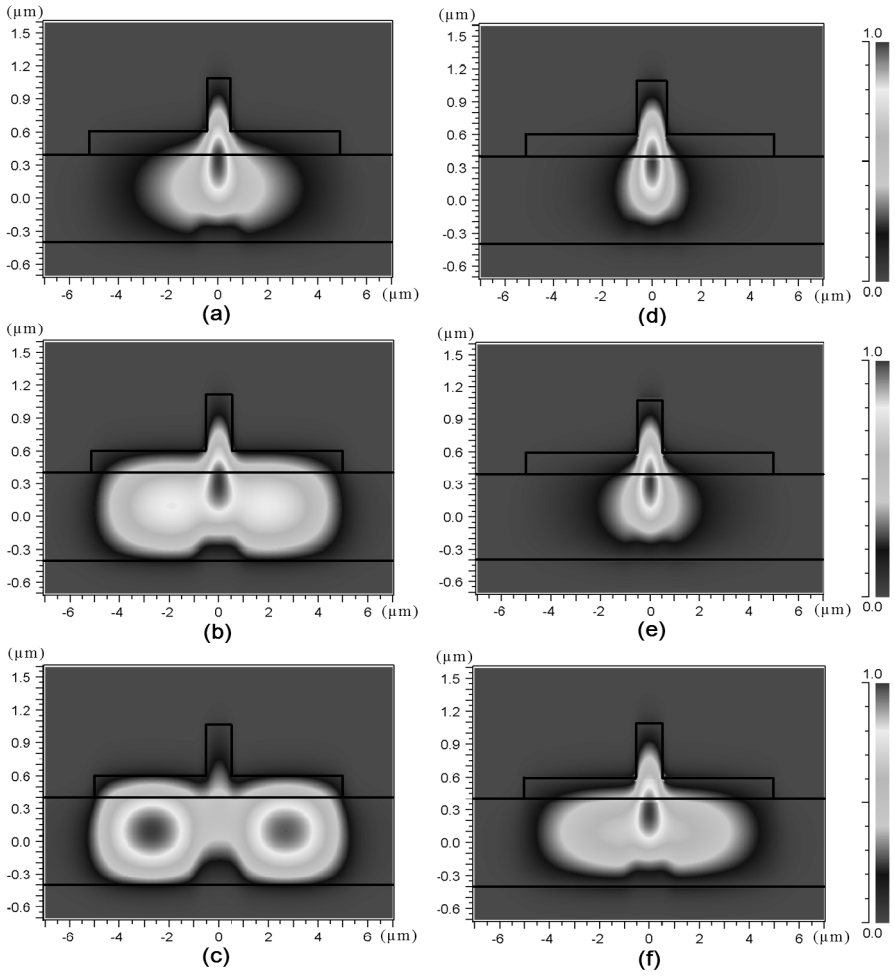

Fig. 7. Mode profiles at λ = 1.55μm, TE mode (a) V_{BE} = 0V (b) V_{BE} = 1.5V (c) V_{BE} = 2.5V; TM mode (d) V_{BE} = 0V (e) V_{BE} = 1.5V (f) V_{BE} = 2.5V

In order to characterize the modulation efficiency, we need to analyze the effective index change Δn_{eff} as a function of V_{BE}. The effective index change is defined as $\Delta n_{eff}(V_{BE}) = n_{eff}(V_{BE}) - n_{eff}(V_{BE} = 0)$. We plot Δn_{eff} as a function of V_{BE} at λ = 1.55μm in Fig. 8. We also include the TM mode at λ = 1.3μm to compare the modulation efficiency at different wavelengths. Larger Δn_{eff} is observed for the TM mode at λ = 1.55μm, which is consistent with the previous analysis of mode profile. By comparing the TM mode at λ = 1.55μm and λ = 1.3μm, we find much stronger effective index changes at λ = 1.55μm. This is primarily because of the larger coefficients in Eq. (1)(a). An expected trend in Fig. 8 is the reduced slope of Δn_{eff} at high V_{BE}. This is a combined outcome of highly localized carrier distribution, saturated carrier injection, and the optical field expansion. The worst case among the three in Fig. 8 is the TE mode at λ = 1.55μm. This is because TE mode per se is less confined than TM mode, and its spatial enlargement is more severe than TM mode as V_{BE} increases.

#110744 - $15.00 USD Received 29 Apr 2009; revised 10 Jul 2009; accepted 13 Jul 2009; published 20 Jul 2009

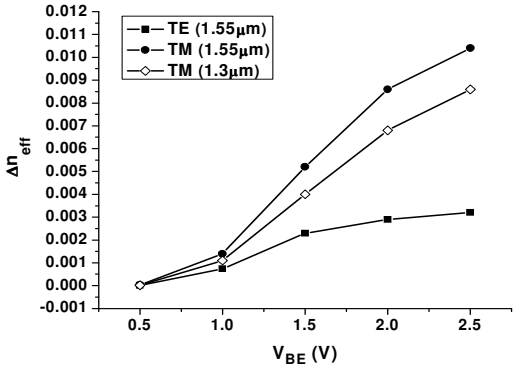

Fig. 8. Δn_{eff} as a function of V_{BE}

In a length-fixed EO modulator, the performance is usually represented by the voltage required for π phase shift (V_π). In our work, since we investigate device behavior by sweeping the voltage, we use the interaction length required for π phase shift (L_π) as an alternative to characterize the performance. L_π is calculated using Eq. (3) [7]:

$$L_\pi = \frac{\lambda_0}{2\Delta n_{eff}} \tag{3}$$

An important figure of merit (FoM) for the EO modulator is the voltage-length product at $\Delta\Phi = \pi$. In the common-emitter configuration of our HBT EO modulator, the FoM corresponds to $V_{BE} \times L_\pi$. At V_{BE} = 2.5V and λ = 1.55μm, L_π for TM mode is 74.5μm, and the FoM is 0.019V-cm. For TE polarization, the results are L_π = 242.2μm and FoM = 0.061V-cm, respectively. A comparison of reported silicon EO modulators in recent years with this work is listed in Table 1. Compared to other EO modulators without incorporating resonator structures, the proposed device exhibits better overall performance, i.e. sub-nanosecond switching delay, less than 100μm L_π, and decent FoM. The combination of small L_π and sub-nanosecond t_s is achieved because of the composition graded thin base, which allows fast carrier transport at high density level. Detailed discussion of t_s will be presented in next section.

Table 1. Comparison of Reported Silicon EO Modulator in Recent Years (t_s is the total switching time, length refers to the active component length, and FCAM is the acronym for free carrier absorption modulator)

Year	Author	Electrical Structure	Optical Structure	t_S (ns)	Length (μm)	FoM (V-cm)
2003	Sciuto et al. [23]	BMFET	FCAM	-	400	-
2003	Png et al [24]	p-i-n	MZI	0.51	500	-
2003	C.Barrios et al. [15]	p-i-n	F-P	1.3	10	8.7×10^{-4}
2004	Liu et al. [7]	MOS	MZI	~0.6	10000	~8
2005	Liao et al. [25]	MOS	MZI	~0.1	3500	3.3
2005	Y.Jiang et al. [9]	p-i-p	PC MZI	-	80	6×10^{-5}
2007	Q.Xu et al. [26]	p-i-n	Ring Resonator	0.3	~10	-
2007	S.Manipatruni et al. [27]	PINIP	Ring Resonator	0.025	~10	-
2007	W.Green et al. [31]	p-i-n	MZI	-	100-200	0.036
2007	F.Gardes et al. [28]	pn	MZI	0.036	5000	2.5
2009	this work	HBT	MZI	0.36	~75	0.019

#110744 - $15.00 USD Received 29 Apr 2009; revised 10 Jul 2009; accepted 13 Jul 2009; published 20 Jul 2009

In this work, we chose a finite S_B and adopted a much larger germanium composition gradient in the base. Comparing with the calculation in our previous research [29], the device model of this work is closer to the physical parameters of the real devices although large geometric dimensions are used. In order to investigate the interaction between the localized free carrier plasma and the light wave in the waveguide more accurately, we used much finer and non-uniform grid when generating the index data file.

We also examined how the carrier plasmas in the emitter and collector affect the EO modulation efficiency. This is done by comparing L_π calculated above with conditions in which the refractive index of the emitter and collector is fixed at its V_{BE} = 0V value. For example, for TM mode at λ = 1.55μm under the bias of V_{BE} = 2.5V, we obtain L_π = 76.7μm without considering carrier plasma in the emitter. A similar investigation not considering index variation in collector produces L_π = 75.2μm. In this condition, the modulation efficiency has 3% contribution from the emitter due to the hole injection, and 0.9% from the collector due to the base widening. These results are consistent with the 1D carrier distribution plot in Fig. 4 and the 2D refractive index map in Fig. 5. Therefore, we can conclude the performance of the HBT EO modulator heavily relies on the carrier plasmas generated in the base region. In the device design, consequently, we can minimize the base widening effect and further compress the hole injection from base into the emitter in order to get faster switching speed.

We calculated the attenuation of the HBT EO modulator according to Eq. (1). Though high attenuation is held for device with heavy doping, the significant reduction in L_π allows the total attenuation of the designed HBT EO modulator to be comparable to other types of silicon EO modulators. For example, at λ = 1.55μm and V_{BE} = 2.5V, the optical loss for TM mode is 3.9dB for an active waveguide length of L_π = 74.5μm. This value is even smaller than reported results from many other work [18,30].

4. Dynamic response considerations

The transient response of the EO modulator refers to switching the device from "ON" to "OFF" or verse vice. It is affected collectively by several mechanisms, namely the carrier diffusion, depletion capacitances charging/discharging time, and the RC delay from the parasitic capacitances and resistances. In general, carrier redistribution is the dominant delay component, especially when the voltage swing is large. This delay can be represented by the forward transit time t_F as expressed in Eq. (4). t_F is the sum of the emitter diffusion time t_E, the base transit time t_B, the emitter-base depletion region transit time t_{BE}, and the base-collector depletion region transit time t_{BC}, and is expressed as [31]

$$t_F = t_E + t_B + t_{BE} + t_{BC} \approx t_E + t_B + t_{BC} = \frac{w_B^2}{\eta D_n} + \frac{w_E w_B}{\theta D_n} + \frac{w_{dBC}}{2v_s} \tag{4}$$

where W_E and W_B are the emitter and the base width, respectively; W_{dBC} is collector depletion region width; v_s is electron drift velocity; D_n is electron diffusion coefficient; η is a factor related to built-in electric field, and θ is coefficient usually between 2 and 5 [21]. In the above expression, t_{BE} is neglected due to the small emitter-base depletion region width. The field factor η is determined by both non-uniform doping and SiGe composition gradient [21], and it can be estimated by

$$\eta \approx 2\left[1+\left(\frac{\varepsilon_{bi}}{\varepsilon_0}\right)^{3/2}\right] \tag{5}$$

where $\varepsilon_0 = 2kT/qW_B$, and ε_{bi} is the built-in field. In this design, η, as a result sorely from SiGe composition gradient is calculated to be 6. It is evident, according to Eq. (4), that t_F is strongly affected by the vertical dimensions of the device. However, t_F only accounts for part of the total delay. Thus, a numerical analysis is necessary to estimate the switching speed of the proposed device.

#110744 - $15.00 USD Received 29 Apr 2009; revised 10 Jul 2009; accepted 13 Jul 2009; published 20 Jul 2009

The transient analysis is performed with MEDICI by switching the base-emitter bias V_{BE} between −1.5V and 2.5V with a 1ps ramp time. The collector current density I_C verse time is assessed to characterize the switching speed, and is plotted in Fig. 9. The rise time that measures the carrier building up process, is 0.21ns. The fall time, or the carrier removal time, is 0.15ns. Evaluated according to the longer delay process, i.e., the turn-on delay, this device supports up to 2.4Gbps data rate for rectangular non-return to zero (NRZ) pulse train. Although carrier injection type of EO modulator is typically considered slow unless an optical resonant structure is used [4], we demonstrated in this work that Multi-GHz switching speed is possible due to the thin base and the built-in electric field.

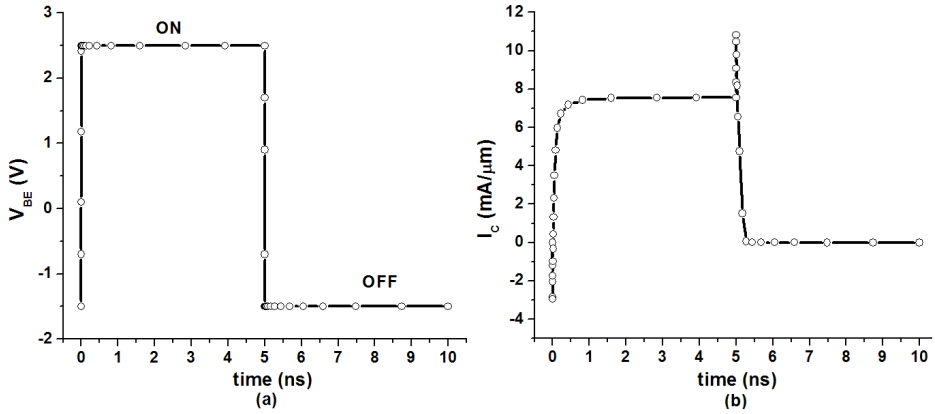

Fig. 9. Transient analysis: (a) input pulse V_{BE}, and (b) I_C response.

5. Discussion of device design strategy

In this work, the device geometry parameters are chosen to maximize the modulation efficiency, and the switch speed is secondary in the design consideration. We first investigated how the mode profile varies with rib waveguide cross-section dimensions, emitter thickness W_E, and the base region width S_B. The geometry parameters that lead to single mode operation of the rib waveguide are determined. Next, we slightly adjusted the emitter thickness as well as the base thickness W_B to maximize the carrier plasma overlap with the optical field. It turns out that the base thickness is the most influential parameter in determining the interaction length L_π and the switching speed. A trade-off between the modulation efficiency and the switching speed is observed.

There are several aspects in this design that distinguish the HBT EO modulator from other approaches. First, the composition graded SiGe base induces a built-in electric field that facilitates carrier transport across the thin base, making the HBT device inherently fast. Second, the proposed HBT EO modulator attains plasma manipulation by carrier injection. Thus, it exhibits much higher modulation efficiency compared to PN junction or MOS based EO modulators. Third, the proposed device provides an extra degree of freedom in device operation because of the use of the third terminal compared to two-terminal devices such as PN and PIN EO modulators. The third terminal can be used to manipulate the electric field profile in the device in order to maximize the overlap between the optical mode and the plasma cloud [18].

6. Conclusions

In this paper, we discussed the optical and electrical characteristics of a SiGe HBT EO modulator with composition graded SiGe base. The strong carrier injection in the base provides very high modulation efficiency. It also has a considerable impact on the mode profile of the HBT waveguide. In this device, the interaction length for a phase shift of π is L_π = 74.5μm for TM mode at λ = 1.55μm. The propagation loss for L_π = 74.5μm is 3.9dB. This device is expected to operate at a switching speed of 2.4GHz or higher. The results are

#110744 - $15.00 USD Received 29 Apr 2009; revised 10 Jul 2009; accepted 13 Jul 2009; published 20 Jul 2009

obtained in a device with a waveguide cross-section larger than 1μm. We expect enhanced modulation efficiency and ultra-fast dynamic response in an optimized submicron HBT EO modulator.

#110744 - $15.00 USD Received 29 Apr 2009; revised 10 Jul 2009; accepted 13 Jul 2009; published 20 Jul 2009